ADVANCED MATERIALS

www.advmat.de

Activated Electron-Transport Layers for Infrared Quantum Dot Optoelectronics

*Jongmin Choi, Jea Woong Jo, F. Pelayo García de Arquer, Yong-Biao Zhao, Bin Sun, Junghwan Kim, Min-Jae Choi, Se-Woong Baek, Andrew H. Proppe, Ali Seifitokaldani, Dae-Hyun Nam, Peicheng Li, Olivier Ouellette, Younghoon Kim, Oleksandr Voznyy, Sjoerd Hoogland, Shana O. Kelley, Zheng-Hong Lu, and Edward H. Sargent**

Photovoltaic (PV) materials such as perovskites and silicon are generally unabsorptive at wavelengths longer than 1100 nm, leaving a significant portion of the IR solar spectrum unharvested. Small-bandgap colloidal quantum dots (CQDs) are a promising platform to offer tandem complementary IR PV solutions. Today, the best performing CQD PVs use zinc oxide (ZnO) as an electron-transport layer. However, these electrodes require ultraviolet (UV)-light activation to overcome the low carrier density of ZnO, precluding the realization of CQD tandem photovoltaics. Here, a new sol–gel UV-free electrode based on Al/Cl hybrid doping of ZnO (CAZO) is developed. Al heterovalent doping provides a strong n-type character while Cl surface passivation leads to a more favorable band alignment for electron extraction. CAZO CQD IR solar cell devices exhibit, at wavelengths beyond the Si bandgap, an external quantum efficiency of 73%, leading to an additional 0.92% IR power conversion efficiency without UV activation. Conventional ZnO devices, on the other hand, add fewer than 0.01 power points at these operating conditions.

Dr. J. Choi, Dr. J. W. Jo,[+] Dr. F. P. García de Arquer, Dr. Y.-B. Zhao, Dr. B. Sun, Dr. J. Kim, Dr. M.-J. Choi, Dr. S.-W. Baek, A. H. Proppe, Dr. A. Seifitokaldani, Dr. D.-H. Nam, O. Ouellette, Dr. Y. Kim,[++] Dr. O. Voznyy, Dr. S. Hoogland, Prof. E. H. Sargent
Department of Electrical and Computer Engineering
University of Toronto
10 King's College Road, Toronto, Ontario M5S 3G4, Canada
E-mail: ted.sargent@utoronto.ca

Dr. Y.-B. Zhao, P. Li, S. Hoogland, Prof. Z. H. Lu
Department of Materials Science and Engineering
University of Toronto
184 College Street, Toronto, Ontario M5S 3E4, Canada

A. H. Proppe, Prof. S. O. Kelley
Department of Chemistry
University of Toronto
80 St. George Street, Toronto, Ontario M5S 3G4, Canada

Prof. S. O. Kelley
Department of Pharmaceutical Sciences
Leslie Dan Faculty of Pharmacy
University of Toronto
Toronto, Ontario M5S 3M2, Canada

[+]Present address: Department of Energy and Materials Engineering, Dongguk University-Seoul, 04620 Seoul, Republic of Korea

[++]Present address: Convergence Research Center for Solar Energy, Daegu Gyeongbuk Institute of Science and Technology, Daegu 42988, Republic of Korea

DOI: 10.1002/adma.201801720

Colloidal quantum dots (CQDs) are promising semiconductor materials owing to their size-tunable bandgap, solution processing, and ambient stability.[1–3] With these benefits, CQDs are widely applied in thin-film optoelectronic devices such as photodetectors,[4,5] transistors,[6,7] light-emitting diodes,[8,9] and photovoltaics (PVs).[10–13] The performance of PbS CQD PVs has been substantially improved so that today they achieve a power conversion efficiency (PCE) of 12%. This has been accomplished via advances in synthesis, ligand exchange, passivation, interface engineering, and device fabrication.[10–17]

The size-tunable bandgap of CQDs provides an opportunity to harvesting the near infrared (IR) region of solar spectrum.[18] Since the absorption onset of abundant light-absorbing materials including perovskite and silicon is shorter than 1100 nm,[19,20] small bandgap (below E_g = 1.1 eV) CQDs are attractive for tandem solar cells that harvest IR light. In the limit of idealized performance, small bandgap ($\approx E_g$ = 0.95 eV) PV can produce a PCE up to 42% when it is combined with wide bandgap ($\approx E_g$ = 1.6 eV) PVs in a tandem solar cell,[21] representing a promising strategy to supplement a performance of wide bandgap PVs.

The most efficient PbS CQD PV devices consist of a planar heterojunction comprising the CQD light-absorbing layer, an n-type metal oxide semiconductor to establish a depletion region in the CQD,[12–17] and a hole-transport layer consisting of thiol-treated CQDs. Zinc oxide (ZnO) nanoparticles are the most widely used material as the n-type semiconductor due to their ease of processing and their suitable electron affinity.[12–17]

Despite these benefits, ZnO exhibit an important drawback: the requirement of ultraviolet (UV)-light-activation for efficient operation. UV activation is a well-known feature of ZnO and it has been reported that UV irradiation on ZnO (UV activation) leads improved device performance.[22–24] This UV activation is thought to provoke photodesorption of nonlattice oxygen on the ZnO surface, leading to increased n-doping and improved conductivity.[23,24]

Whereas UV activation is not an issue in standalone CQD PV, it becomes a fundamental limitation for IR CQD PV applications and tandem solar cell configurations. Another

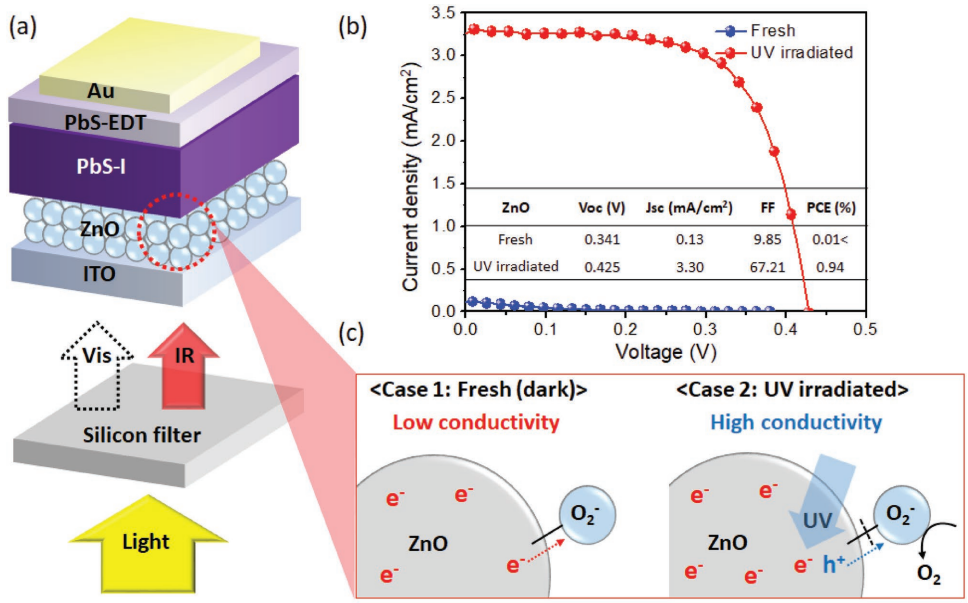

Figure 1. UV activation issues of ZnO ETL in IR CQD PV. a) Schematic illustration of device architecture for IR CQD PV and b) corresponding current density–voltage (*J–V*) characteristics of device prepared using ZnO electron-transport layer (ETL) and 1.05 eV bandgap PbS under 1100 nm long-wave-pass silicon filtered AM 1.5G solar illumination according to UV activation. c) Schematic illustration of the nonlattice oxygen adsorption–desorption process according to UV activation and corresponding predicted electrical conductivity of ZnO.

limitation of ZnO in IR CQD PV is its unfavorable band alignment with a small bandgap CQD layer, which can result in poor electron collection. CQD absorption beyond 1100 nm require larger dot sizes, and the conduction band (CB) level of iodide-treated CQDs becomes deeper (below 4.4 eV) with increasing size.[25,26] In light of the CB level of ZnO around 4.1 eV,[17,27] this leads to poor charge injection and to a significant rate of interfacial charge recombination.[28–30]

The development of UV-activation-free electron-transport layers (ETLs) with favorable band alignment for electron collection is therefore important to realizing highly efficient IR CQD PV. Al is a well-known n-type dopant for metal oxides to increase free carrier density, resulting in enhanced conductivity,[31,32] and it can therefore potentially reduce the UV-activation problem in ZnO. However, previous Al doped ZnO (AZO) electrodes were generally produced by vacuum processing, which may limit their large-area manufacture. Moreover, previously reported AZO films exhibit an unfavorable CB level (around 4.1 eV) limiting electron collection from the small bandgap CQD layer.[33]

To address these issues, we developed a solution-processed Al/Cl hybrid doped ZnO (CAZO) electrodes. We found that the well-defined CAZO electrodes show high conductivity regardless of UV activation, and they also exhibit deep CB level (around 4.5 eV) which is favorable for electron extraction. In IR CQD PVs, CAZO devices demonstrate an IR external quantum efficiency (EQE) of 73%, leading to a PCE of 0.92% under silicon-filtered (to cutoff under 1100 nm light) AM 1.5 light without UV activation; conventional ZnO devices, on the other hand, show negligible PCEs (<0.01%) at the same conditions.

To characterize the role of UV activation in conventional ZnO as applied in IR CQD PV, ZnO nanoparticles were used as the ETL in a device configuration consisting of indium tin oxide (ITO)/ZnO nanoparticles/PbS-I (lead-halide-passivated PbS)/1,2-ethanedithiol (EDT)-treated PbS/Au (**Figure 1**a). For device fabrication, ZnO nanoparticles were spin-cast onto cleaned ITO glass, and a 1.05 eV bandgap PbS-I layer was spin coated onto the ZnO film leading to a 250 nm film PbS thickness (Figure S1, Supporting Information). The hole-transport layer consists of two layers of PbS exchanged with EDT in a layer-by-layer fashion (see the Experimental Section for more details). To evaluate the IR device performance as a silicon-back cell, an 1100 nm long-wave-pass filter was placed in front of the CQD PV device. Figure 1b shows *J–V* characteristics of ZnO used device under Si-filtered AM 1.5G solar illumination before and after UV activation on device (the full AM 1.5G spectrum PCE without silicon filter and corresponding EQE spectra were shown in Figure S2, Supporting Information). These results indicate the need of UV-activation problem in ZnO. The IR PCE of UV-activated devices reaches 0.94%; while, without UV activation, the devices reach only 0.01% PCE. Histograms of the photovoltaic performance of IR CQD solar cells fabricated with ZnO after UV activation are shown in Figure S2 in the Supporting Information.

We hypothesized that the main factor behind the need of UV activation is the different conductivity of ZnO before/after UV activation. It is reported that the fresh ZnO before UV activation contains chemisorbed nonlattice oxygen on the surface, which can extract free electrons from ZnO leading to a low conductivity.[22,23,34] In contrast, under UV activation, photoexcited holes might migrate to capture electrons from chemisorbed nonlattice oxygen species; and the chemisorbed nonlattice oxygen become then discharged and detached from ZnO surface[22,23] (Figure 1c).

The conductivity is governed by carrier concentration and electron mobility. We sought therefore to introduce

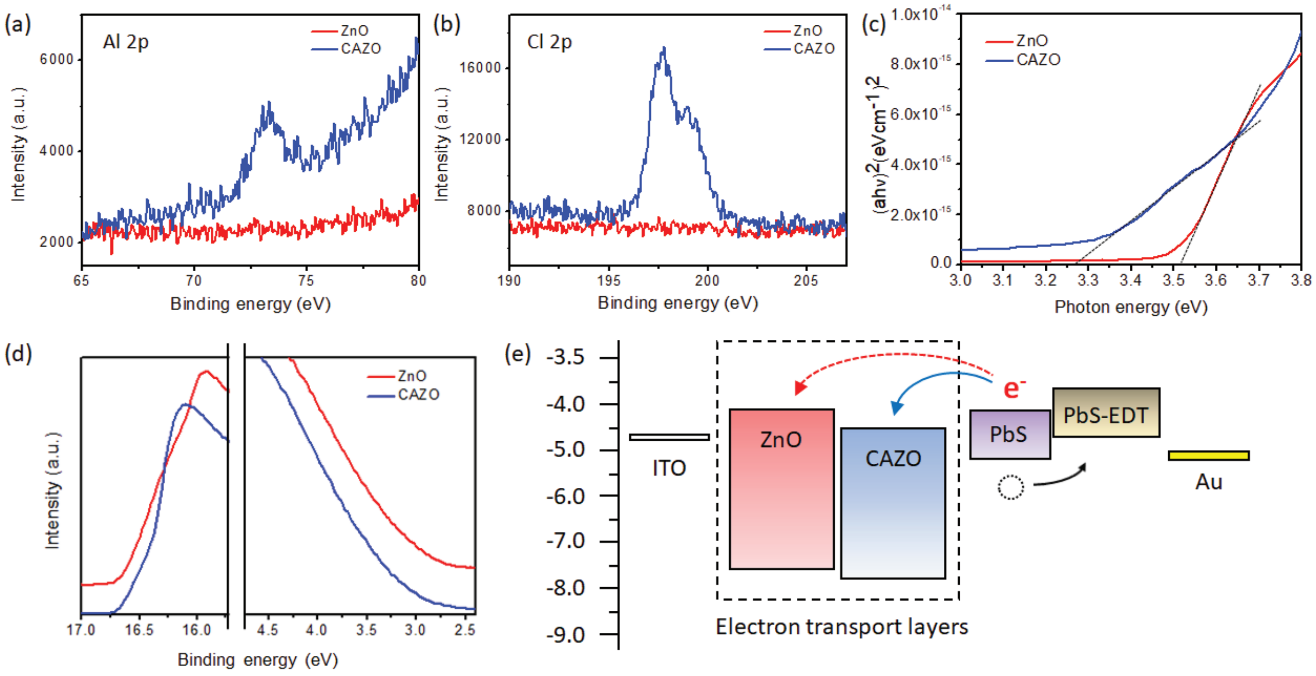

Figure 2. Electrical characteristics of Al and Cl codoped ZnO (CAZO) film. a) Al 2p and b) Cl 2p X-ray photoelectron spectroscopy (XPS) spectra of ZnO and CAZO films. c) Tauc plots of ZnO and CAZO films on glass. d) Cutoff and onset region of UPS spectra for ZnO and CAZO films on ITO glass. e) Schematic band alignment diagram of ZnO and CAZO determined from optical bandgap and UPS analysis.

n-type dopants such as Al into ZnO lattice during synthesis, seeking to improve the film conductivity due to increased carrier concentration.[35] We further took the view that the incorporation of halide species such as Cl into ZnO would shift down the CB due to the strong electron-withdrawing nature of the halides.[17,36]

We sought therefore to develop Al/Cl doped ZnO (CAZO) electrodes that are UV activation free. We used an $AlCl_3$ precursor to synthesize CAZO based on a modified sol–gel method.[32] X-ray photoelectron spectroscopy (XPS) was employed to investigate the binding affinity of Al and Cl to ZnO. The Al 2p and Cl 2p spectra of the ZnO layers shown in **Figure 2**a,b demonstrate the incorporation of Al and Cl into CAZO film. To evaluate the electronic energy band alignment of CAZO, we acquired Tauc plots and ultraviolet photoelectron spectra (UPS). The Tauc plot of CAZO film (Figure 2c, obtained from the optical absorption spectra of ZnO films on the glass as shown in Figure S3, Supporting Information) indicates that the optical bandgap of CAZO (3.3 eV) narrows compared to that (3.52 eV) of ZnO films—an effect of Al doping. It is reported that the hybridization between states of the ZnO and of the Al dopant can yield new electronic donor states below lowest edge of the CB, resulting in narrowing CB of ZnO.[37] From UPS spectra shown in Figure 2d (obtained from full UPS spectra shown in Figure S4, Supporting Information), we found that the CAZO films show a downward shift (from 7.62 to 7.82 eV) of the valence band level, similar to observations in Cl incorporated metal oxides.[17,36] Figure 2e shows the band alignment diagram of ZnO and CAZO deduced from the optical bandgaps (Figure 2c) and the UPS results (Figure 2d). The deep electron affinity of CAZO is beneficial for electron extraction from the CQD layer.

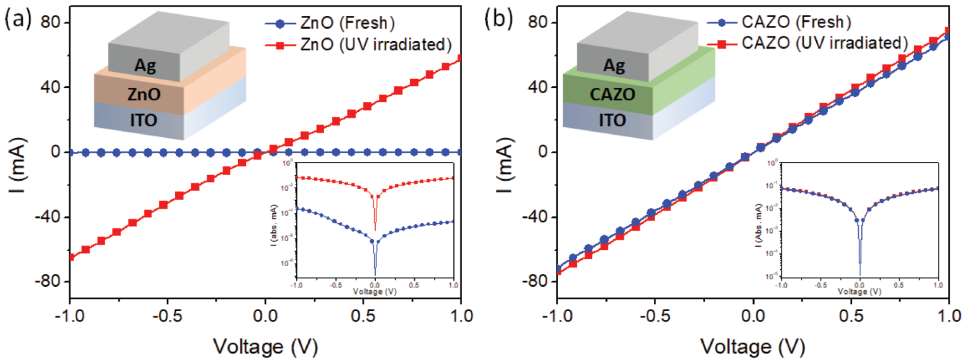

Figure 3. Conductivity study of ZnO and CAZO under dark and illumination. *I–V* curves (with log scale *I–V* inset) of the devices for a) ITO/ZnO (100 nm)/Ag and b) ITO/CAZO (100 nm)/Al in the dark and under 1000 W m^{-2} AM 1.5G illumination.

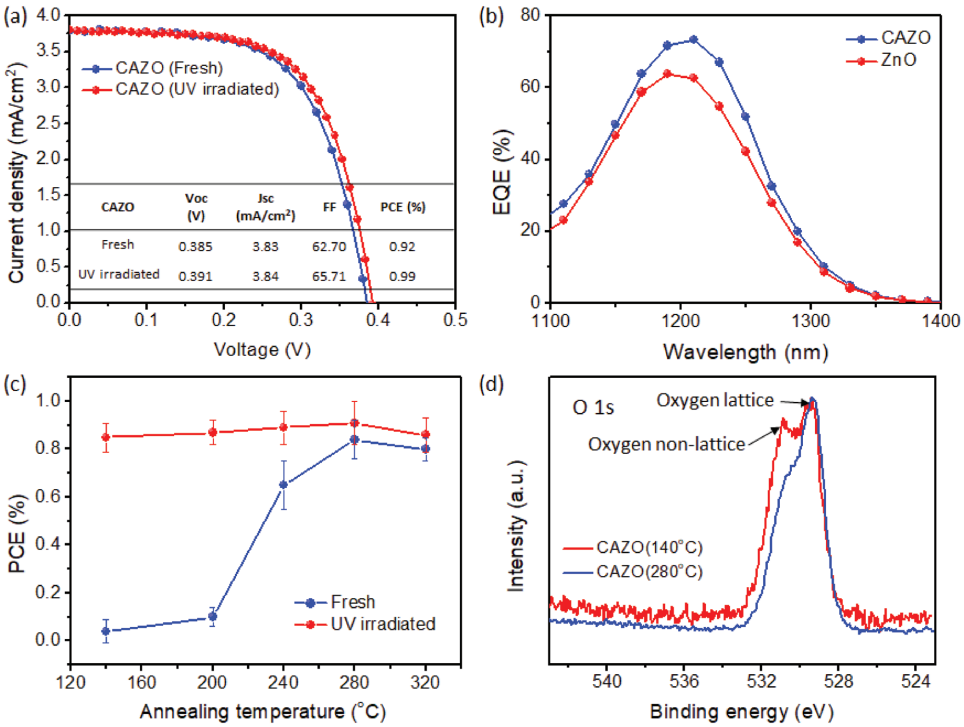

Figure 4. The effect of CAZO on IR CQD solar cell performance. a) Current density–voltage (*J–V*) characteristics of IR CQD PV devices prepared using CAZO ETL and 1.05 eV bandgap PbS under silicon filtered AM 1.5G solar illumination according to UV activation. b) EQE spectra of IR CQD PV prepared with ZnO and CAZO films. c) Si filtered PCE values of IR CQD PV prepared with different annealed CAZO films according to UV activation. d) O 1s XPS spectra of low (140 °C) and high (280 °C) temperature annealed CAZO films.

Figure 3 shows *I–V* characteristics of the devices for ITO/ETLs (ZnO or CAZO)/Ag in the dark and under AM 1.5G illumination to verify the doping effect on conductivity. Reference devices using ZnO films showed diode behavior with low dark currents (electrical conductivity of ZnO films in the dark is ≈4.24×10^{-7} S m^{-1}, Figure S5, Supporting Information), whereas the *I–V* curve became linear in relation to the high current under illumination as shown in Figure 2a. The *I–V* curve transition indicated that the ZnO film changed from semiconductor in the dark to conductor after UV activation with the electrical conductivity of ≈1.31×10^{-3} S m^{-1}. The different behaviors of ZnO films in dark and under illumination illustrate the distinct *J–V* features of IR CQD PV devices before/after UV activation (Figure 1b). In contrast, devices based on CAZO films displayed similar conductivity in the dark and under illumination with an electrical conductivity under dark/light of ≈1.44×10^{-3} and ≈1.49×10^{-3} S m^{-1}, respectively. The high conductivity of CAZO film in the dark can be explained in terms of the increased carrier concentration by Al doping. The significantly improved conductivity of CAZO under dark supports the UV-activation-free *J–V* behavior of the IR CQD PVs.

We then delved into the effect of CAZO over ZnO in IR CQD PV applications. A similar device architecture was employed (ITO/CAZO or ZnO/PbS-I/EDT-treated PbS/Au). We found that highly doped CAZO leads to slightly decreased V_{oc} compared to ZnO samples. An optimized Al doping concentration is observed ≈1 atomic percent (at%) as shown in Figure S6 in the Supporting Information. The best-performing devices with CAZO exhibited a superior filtered PCE of 0.99% following UV activation (**Figure 4**a, the full AM 1.5G spectrum PCE without silicon filter and corresponding EQE spectra were shown in Figure S7, Supporting Information) compared to a 0.94% for ZnO devices (Figure 1b). The main contribution to the improved PCE in the CAZO device is the enhanced J_{sc} (from 3.30 to 3.84 mA cm^{-2}), a consequence of a better extraction of photoexcited electrons in the CQD layer due to the effect of Cl (Figure 2e).

The notably improved EQE of CAZO devices (≈73%) at the ≈1200 nm exciton peak compared to that (≈64%) of ZnO agrees well with result of J_{sc} (Figure 4a,b). ZnO- and CAZO-based devices exhibited similar long-term stability, retaining over 90% of their initial filtered PCE following 300 h of storage in air (Figure S8, Supporting Information). Notably, CAZO devices are operated without UV activation whereas ZnO devices require UV activation before each run. The obtained filtered PCE from CAZO without UV activation is 0.92% (Figure 4a, histograms of IR CQD solar cells fabricated with CAZO following UV activation are shown in Figure S9, Supporting Information). The CAZO-based devices exhibited superior photostability compared to standard ZnO devices (Figure S10, Supporting Information) and retained over 90% of their initial PCE following 14 h operation. ZnO devices, in contrast, exhibited 40% relative PCE degradation over the same operating time. We ascribed the lower photostability of ZnO to the continuous requirement of UV activation due to oxygen readsorption.[23] The PCEs of both ZnO- and CAZO-based devices recovered to their initial values following dark storage.

In addition, we found that the annealing temperature of CAZO is critical for reducing UV activation in the device. Low temperature annealed (≈140 °C) CAZO exhibited a huge gap of device performance depending on UV activation (Figure 4c), similar to that found for ZnO. The need of UV activation decreases with increasing annealing temperature and becomes negligible for temperatures above 280 °C.

To shed light on the origins of this temperature dependence, we carried out elemental analysis based on X-ray spectroscopies. The O 1s XPS spectra (Figure 4d) reveal that the different operating behavior of devices as a function of the annealing temperature of CAZO can be understood in terms of different surface functionality of ZnO films. The lower-binding-energy peak (≈529 eV) of O 1s XPS spectra is attributed to oxygen atoms in the ZnO lattice, whereas the higher-binding-energy (≈531 eV) of O 1s XPS spectra is associated with nonlattice adsorbed oxygen. Low-temperature-annealed CAZO films exhibited a significantly higher fraction of higher binding-energy components compared to high temperature annealed CAZO films. A high concentration of nonlattice oxygen can hinder electron transport, leading to low conductivity in the absence of UV activation (Figure 1c). These results indicate that not only the increased free carrier density but also the decreased amount of nonlattice oxygen are valuable in diminishing the UV-activation problem in ZnO.

In summary, we developed a UV-activation-free ETL for IR CQD PV via Al and Cl hybrid doping on ZnO. The UV-activation problem arises from the conductivity of ZnO, which we improved by controlling the amount of free carrier and nonlattice oxygen in ZnO. CAZO electrodes exhibited a favorable band alignment for electron extraction due to surface Cl, and a high intrinsic conductivity regardless of UV activation due to the heterovalence incorporation of Al. With these benefits, the IR CQD PVs based on CAZO exhibit an IR EQE beyond the Si bandgap of 73%, leading to the addition of 0.92% PCE points. Conventional ZnO-based devices showed negligible PCEs at the same conditions. This work provides important insights into achieving UV-activation-free metal oxide for IR and tandem optoelectronic devices.

Experimental Section

Preparation of CAZO and ZnO Films: $Zn(Ac)_2{\cdot}2H_2O$ (0.44 g) and $AlCl_3$ (2.6 mg) were mixed in 20 mL of ethanol. The mixed solution was heated 80 °C for 2 h and afterward filtered through a 0.45 µm filter to remove insoluble debris. The filtered solution immediately spin coated (5000 rpm for 30 s) on cleaned ITO glass (to prevent precipitation of $Zn(Ac)_2{\cdot}2H_2O$ due to lack of stabilizer such as ethanolamine) and heated at 280 °C for 20 min for conversion of the precursors to CAZO via hydrolysis. The process including deposition and heating was repeated two times. The ZnO film was prepared by spin coating (5000 rpm for 30 s) of ZnO nanoparticles on ITO glass and the solution of ZnO nanoparticles was synthesized following a reported method.[13]

Synthesis of PbS CQDs: Lead halide-passivated PbS CQDs were synthesized by solution-phase ligand-exchange process with oleic-acid-capped CQDs (OA-CQDs) as described in previous literature.[13] The solution-phase ligand-exchange was performed by following reported method for IR CQD inks.[38] In detail, solution of lead halides (0.5 mmol PbI_2 and 0.11 mmol $PbBr_2$) and 0.21 mmol NaAc dissolved in 5 mL dimethylformamide (DMF) was prepared for ligand exchange, and mixed with 5 mL of OA-CQDs (7 mg mL^{-1} in octane). The mixed solution was vortexed for 5 min at room temperature to complete transfer of CQD toward DMF. The ligand-exhanged solution was washed three times with octane for removing remained residues. The washed CQDs precipitated by addition of 0.3 mL toluene, and the CQDs were totally separated by following centrifugation. After 10 min drying under vacuum, the CQDs were redispersed in butylamine (BTA) with desired concentrations for film deposition.

Fabrication of IR CQD Solar Cells: The lead halide passivated-PbS IR-CQDs dissolved in BTA: DMF (4:1 v/v) mixtures were spin coated (2500 rpm for 30 s) on as-prepared ETL films (ZnO and CAZO). After that, EDT-treated PbS layer was spin coated on the lead halide passivated-CQD layer following previously reported method. For the top electrode, 120 nm Au was thermally evaporated on the PbS CQD film.

J–V Characterization and EQE Measurements: Photovoltaic performances of the devices were determined using Keithley 2400 source under AM 1.5G illumination (Sciencetech class 3A) of 100 mW cm^{-2} with 1100 nm long-wave-pass silicon filter in N_2 atmosphere. An aperture (active area 0.049 cm^2) was used for measurement. The spectral mismatch was calibrated by a reference solar cell (Newport). It was corrected for spectral mismatch between the lamp and AM 1.5G.[20] EQE spectra were obtained from under monochromatic illumination (400 W Xe lamp equipped with a monochromator and cutoff filters) after the correction of power with Newport 818-UV and Newport 838-IR photodetectors. The current response was obtained with a Lakeshore preamplifier connected to a Stanford Research 830 lock-in amplifier.

Characterization: XPS and UPS spectra of ZnO films are obtained on ITO substrate. Photoelectron spectroscopy was carried out in a PHI5500 Multi-Technique system with monochromatic Al-K_α radiation (XPS) (h_ν = 1486.7 eV) and nonmonochromatized He-I_α radiation (UPS) (h_ν = 21.22 eV). Optical absorption measurements were obtained from a UV–vis–IR spectrophotometer (Lambda 950). Field emission scanning electron microscopy (Hitachi SU8230) was employed for morphological and structural characterization.

Supporting Information

Supporting Information is available from the Wiley Online Library or from the author.

Acknowledgements

J.C., J.W.J., and F.P.G.d.A. contributed equally to this work. The authors thank L. Levina, R. Wolowiec, D. Kopilovic, and E. Palmiano for their help over the course of this research. This research was supported by Ontario Research Fund-Research Excellence program (ORF7-Ministry of Research and Innovation, Ontario Research Fund-Research Excellence Round 7) and by the Natural Sciences and Engineering Research Council (NSERC) of Canada.

Conflict of Interest

The authors declare no conflict of interest.

Keywords

conductivity, doping, Infrared, quantum dot solar cells, ZnO

Received: March 16, 2018
Revised: April 14, 2018
Published online:

[1] S. A. McDonald, G. Konstantatos, S. Zhang, P. W. Cyr, E. J. D. Klem, L. Levina, E. H. Sargent, *Nat. Mater.* **2005**, *4*, 138.
[2] O. E. Semonin, J. M. Luther, S. Choi, H. Y. Chen, J. Gao, A. J. Nozik, M. C. Beard, *Science* **2011**, *334*, 1530.
[3] M. Yuan, M. Liu, E. H. Sargent, *Nat. Energy* **2016**, *1*, 16016.
[4] G. Konstantatos, I. Howard, A. Fischer, S. Hoogland, J. Clifford, E. Klem, L. Levina, E. H. Sargent, *Nature* **2006**, *442*, 180.
[5] J.-S. Lee, M. V. Kovalenko, J. Huang, D. S. Chung, D. V. Talapin, *Nat. Nanotechnol.* **2011**, *6*, 348.
[6] S. Y. Jeong, S. C. Lim, D. J. Bae, Y. H. Lee, H. J. Shin, S.-M. Yoon, J. Y. Choi, O. H. Cha, M. S. Jeong, D. Perello, M. Yun, *Appl. Phys. Lett.* **2008**, *92*, 243103.
[7] S. Yang, N. Zhao, L. Zhang, H. Zhong, R. Liu, B. Zou, *Nanotechnology* **2012**, *23*, 255203.
[8] V. M. Wood, J. Panzer, J. Chen, M. S. Bradley, J. E. Halpert, M. G. Bawendi, V. Bulović, *Adv. Mater.* **2009**, *21*, 2151.
[9] X. Gong, Z. Yang, G. Walters, R. Comin, Z. Ning, E. Beauregard, V. Adinolfi, O. Voznyy, E. H. Sargent, *Nat. Photonics* **2016**, *10*, 253.
[10] A. H. Ip, S. M. Thon, S. Hoogland, O. Voznyy, D. Zhitomirsky, R. Debnath, L. Levina, L. R. Rollny, G. H. Carey, A. Fischer, K. W. Kemp, I. J. Kramer, Z. Ning, A. J. Labelle, K. W. Chou, A. Amassian, E. H. Sargent, *Nat. Nanotechnol.* **2012**, *7*, 577.
[11] Z. Ning, O. Voznyy, J. Pan, S. Hoogland, V. Adinolfi, J. Xu, M. Li, A. R. Kirmani, J. Sun, J. Minor, K. W. Kemp, H. Dong, L. Rollny, A. Labelle, G. Carey, B. Sutherland, I. Hill, A. Amassian, H. Liu, J. Tang, O. M. Bakr, E. H. Sargent, *Nat. Mater.* **2014**, *13*, 822.
[12] C.-H. M. Chuang, P. R. Brown, V. Bulović, M. G. Bawendi, *Nat. Mater.* **2014**, *13*, 796.
[13] M. Liu, O. Voznyy, R. Sabatini, F. P. Garcia de Arquer, R. Munir, A. H. Balawi, X. Lan, F. Fan, G. Walters, A. R. Kirmani, S. Hoogland, F. Laquai, A. Amassian, E. H. Sargent, *Nat. Mater.* **2017**, *16*, 258.
[14] G.-H. Kim, F. P. García de Arquer, Y. J. Yoon, X. Lan, M. Liu, O. Voznyy, Z. Yang, F. Fan, A. H. Ip, P. Kanjanaboos, S. Hoogland, J. Y. Kim, E. H. Sargent, *Nano Lett.* **2015**, *15*, 7691.
[15] X. Lan, O. Voznyy, F. P. García de Arquer, M. Liu, J. Xu, A. H. Proppe, G. Walters, F. Fan, H. Tan, M. Liu, Z. Yang, S. Hoogland, E. H. Sargent, *Nano Lett.* **2016**, *16*, 4630.
[16] H. Aqoma, M. A. Mubarok, W. T. Hadmojo, E.-H. Lee, T.-W. Kim, T. K. Ahn, S.-H. Oh, S.-Y. Jang, *Adv. Mater.* **2017**, *29*, 1605756.
[17] J. Choi, Y. Kim, J. W. Jo, J. Kim, B. Sun, G. Walters, F. P. García de Arquer, R. Quintero-Bermudez, Y. Li, C. S. Tan, L. N. Quan, A. P. T. Kam, S. Hoogland, Z. Lu, O. Voznyy, E. H. Sargent, *Adv. Mater.* **2017**, *29*, 1702350.
[18] H. Choi, J. H. Ko, Y. H. Kim, S. Jeong, *J. Am. Chem. Soc.* **2013**, *135*, 5278.
[19] J.-W. Lee, D.-J. Seol, A.-N. Cho, N.-G. Park, *Adv. Mater.* **2014**, *26*, 4991.
[20] A. H. Ip, A. Kiani, I. J. Kramer, O. Voznyy, H. F. Movahed, L. Levina, M. M. Adachi, S. Hoogland, E. H. Sargent, *ACS Nano* **2015**, *9*, 8833.
[21] A. D. Vos, *J. Phys. D: Appl. Phys.* **1980**, *13*, 839.
[22] C. E. Small, S. Chen, J. Subbiah, C. M. Amb, S.-W. Tsang, T.-H. Lai, J. R. Reynolds, F. So, *Nat. Photonics* **2012**, *6*, 115.
[23] S. Wilken, J. Parisi, H. Borchert, *J. Phys. Chem. C* **2014**, *118*, 19672.
[24] C. Leow, T. Harada, T. Ohnishi, M. Matsumura, *RSC Adv.* **2015**, *5*, 22647.
[25] P. R. Brown, D. Kim, R. R. Lunt, N. Zhao, M. G. Bawendi, J. C. Grossman, V. Bulović, *ACS Nano* **2014**, *8*, 5863.
[26] D. H. Yeon, S. M. Lee, Y. H. Jo, J. Moon, Y. S. Cho, *J. Mater. Chem. A* **2014**, *2*, 20112.
[27] G. Yang, H. Tao, P. Qin, W. Kea, G. Fang, *J. Mater. Chem. A* **2016**, *4*, 3970.
[28] I. Robel, M. Kuno, P. V. Kamat, *J. Am. Chem. Soc.* **2007**, *129*, 4136.
[29] J. P. Correa Baena, L. Steier, W. Tress, M. Saliba, S. Neutzner, T. Matsui, F. Giordano, T. J. Jacobsson, A. R. Srimath Kandada, S. M. Zakeeruddin, A. Petrozza, A. Abate, M. K. Nazeeruddin, M. Grätzel, A. Hagfeldt, *Energy Environ. Sci.* **2015**, *8*, 2928.
[30] J. Choi, S. Song, M. T. Hörantner, H. J. Snaith, T. Park, *ACS Nano* **2016**, *10*, 6029.
[31] T. Stubhan, H. Oh, L. Pinna, J. Krantz, I. Litzov, C. J. Brabec, *Org. Electron.* **2011**, *12*, 1539.
[32] T. Stubhan, I. Litzov, N. Li, M. Salinas, M. Steidl, G. Sauer, K. Forberich, G. J. Matt, M. Halik, C. J. Brabec, *J. Mater. Chem. A* **2013**, *1*, 6004.
[33] Y. Bi, S. Pradhan, S. Gupta, M. Z. Akgul, A. Stavrinadis, G. Konstantatos, *Adv. Mater.* **2018**, *30*, 1704928.
[34] J. Kim, G. Kim, Y. Choi, J. Lee, S. H. Park, K. Lee, *J. Appl. Phys.* **2012**, *111*, 114511.
[35] S.-Y. Kuo, W.-C. Chen, F.-I. Lai, C.-P. Cheng, H.-C. Kuo, S.-C. Wang, W.-F. Hsieh, *J. Cryst. Growth* **2006**, *287*, 78.
[36] H. Tan, A. Jain, O. Voznyy, X. Lan, F. P. Garcia de Arquer, J. Z. Fan, R. Quintero-Bermudez, M. Yuan, B. Zhang, Y. Zhao, F. Fan, P. Li, L. N. Quan, Y. Zhao, Z.-H. Lu, Z. Yang, S. Hoogland, E. H. Sargent, *Science* **2017**, *355*, 722.
[37] M. Gabás, S. Gota, J. R. Ramos-Barrado, M. Sánchez, N. T. Barrett, J. Avila, M. Sacchi, *Appl. Phys. Lett.* **2005**, *86*, 042104.
[38] Y. Kim, F. Che, J. W. Jo, J. Choi, O. Voznyy, F. P. Garcia de Arquer, B. Sun, J. Kim, R. Quintero-Bermudez, F. Fan, C. S. Tan, E. Bladt, G. Walters, A. Proppe, C. Zou, H. Yuan, S. Bals, J. Hofkens, M. B. J. Roeffaers, E. H. Sargent, unpublished.

